nature physics

ARTICLES

PUBLISHED ONLINE: 24 FEBRUARY 2013 | DOI: 10.1038/NPHYS2564

Photoexcitation cascade and multiple hot-carrier generation in graphene

K. J. Tielrooij[1]*, J. C. W. Song[2,3], S. A. Jensen[4,5], A. Centeno[6], A. Pesquera[6], A. Zurutuza Elorza[6], M. Bonn[4], L. S. Levitov[2] and F. H. L. Koppens[1]*

The conversion of light into free electron–hole pairs constitutes the key process in the fields of photodetection and photovoltaics. The efficiency of this process depends on the competition of different relaxation pathways and can be greatly enhanced when photoexcited carriers do not lose energy as heat, but instead transfer their excess energy into the production of additional electron–hole pairs through carrier–carrier scattering processes. Here we use optical pump–terahertz probe measurements to probe different pathways contributing to the ultrafast energy relaxation of photoexcited carriers. Our results indicate that carrier–carrier scattering is highly efficient, prevailing over optical-phonon emission in a wide range of photon wavelengths and leading to the production of secondary hot electrons originating from the conduction band. As hot electrons in graphene can drive currents, multiple hot-carrier generation makes graphene a promising material for highly efficient broadband extraction of light energy into electronic degrees of freedom, enabling high-efficiency optoelectronic applications.

For many optoelectronic applications, it is highly desirable to identify materials in which an absorbed photon is efficiently converted to electronic excitations. The unique properties of graphene, such as its gapless band structure, flat absorption spectrum[1] and strong electron–electron interactions[2], make it a highly promising material for efficient broadband photon–electron conversion[3]. Indeed, recent theoretical work has anticipated that in graphene multiple electron–hole pairs can be created from a single absorbed photon during energy relaxation of the primary photoexcited electron–hole pair[4,5]. A photoexcited carrier relaxes through two competing pathways: carrier–carrier scattering and phonon emission. In the former process the energy of photoexcited carriers remains in the electron system, being transferred to secondary electrons that gain energy (become hot), whereas in the phonon emission process the energy is lost to the lattice as heat. Although recent experiments have shown that photoexcitation of graphene can generate hot carriers[6,7], it remains unknown how efficient this process is with respect to optical-phonon emission.

Here we study the energy relaxation process of the primary photoexcited electron–hole pair in doped single-layer graphene. In particular, we quantify the branching ratio between the two competing relaxation pathways. Given the challenging timescale with which these processes occur, we employ an ultrafast optical pump–terahertz probe measurement technique, where we exploit the variation of the photon energy of the pump light. Changing this photon energy is crucial as it allows us to prepare the system with photoexcited carriers having a prescribed initial energy determined by the photon energy, and follow the ensuing energy relaxation dynamics. We show experimentally, in combination with theoretical modelling, that carrier–carrier scattering is the dominant relaxation process. This process leads to the creation of secondary hot electrons that originate from the conduction band.

We note that assigning a conventional name to a process in which secondary hot carriers are generated by photoexcited carriers in graphene is by no means a trivial matter. This is so because different nomenclature is used in the optical studies of semiconductors and metals: electrons and holes in semiconductors are defined with respect to the conduction and valence bands, whereas in metals the distinction between the states above and below the Fermi level plays the key role. Doped graphene can be viewed as a mixture of both: it is a semimetal with the Fermi level detuned away from the Dirac point. To minimize confusion, and at the same time to make the discussion of our results unambiguous, we will denote the process in question as hot-carrier multiplication. This intraband process is different from conventional carrier multiplication observed in semiconductor systems[8–11] and theoretically predicted for undoped graphene[4,5], where additional electron–hole pairs originate from interband transitions. The generation of secondary hot carriers from the conduction band in doped graphene is a technologically relevant relaxation process because the thermoelectric effect dominates the optoelectronic response of graphene[6,7]. For hot-carrier multiplication, the total number of carriers in the conduction band does not change as a result of carrier–carrier scattering. However, the number of hot carriers (that is, carriers with an energy above the Fermi level) increases. It is through this multiplication of hot electrons in the conduction band that the energy of the primary photoexcited carrier is harvested by the electron subsystem and later used to generate an optoelectronic response.

The employed technique consists of an ultrafast optical pump pulse that excites carriers and a terahertz probe pulse that passes through the sample after a variable delay time (Fig. 1a). The terahertz pulses afford an exquisite time-resolved probe of the high-frequency photoconductive response of photoexcited carriers, as reviewed in ref. 12. This technique has been used before with

[1]ICFO—Institut de Ciéncies Fotóniques, Mediterranean Technology Park, Castelldefels (Barcelona) 08860, Spain, [2]Department of Physics, Massachusetts Institute of Technology, Cambridge, Massachusetts 02139, USA, [3]School of Engineering and Applied Sciences, Harvard University, Cambridge, Massachusetts 02138, USA, [4]Max Planck Institute for Polymer Research, Ackermannweg 10, 55128 Mainz, Germany, [5]FOM Institute AMOLF, Amsterdam, Science Park 104, 1098 XG Amsterdam, Netherlands, [6]Graphenea SA, 20018 Donostia-San Sebastián, Spain. *e-mail: klaas-jan.tielrooij@icfo.es; frank.koppens@icfo.es.

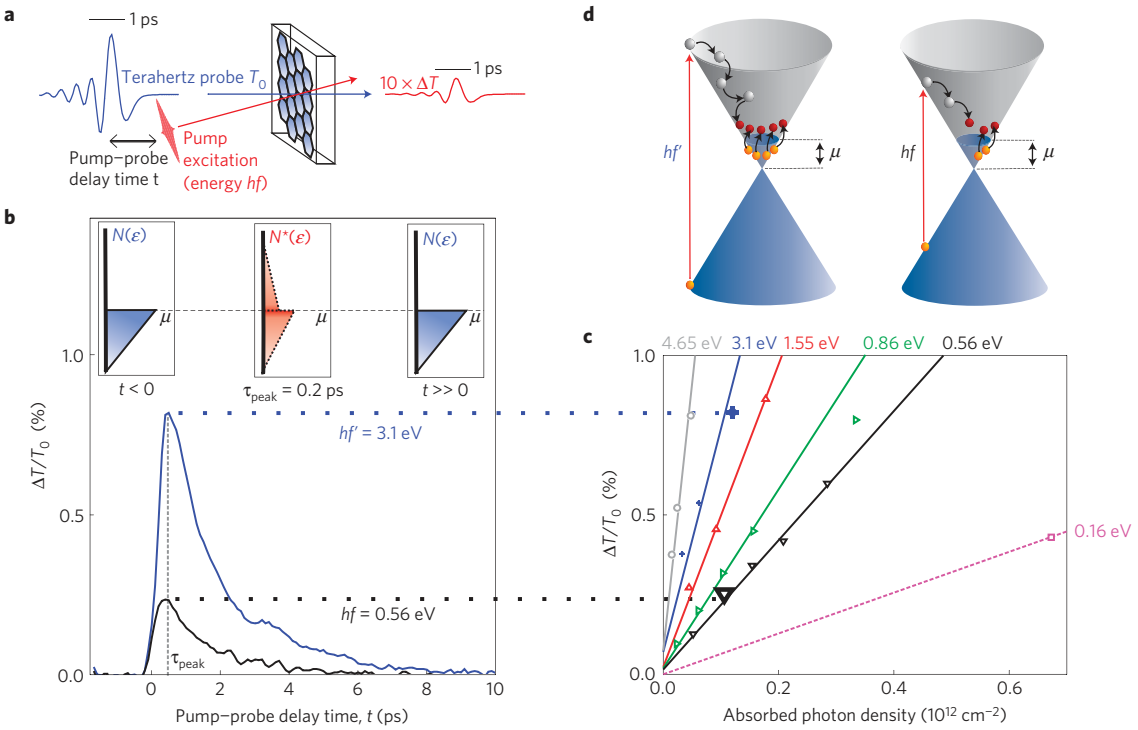

Figure 1 | Experimental realization and results. a, Experimental observation of carrier dynamics. Electron–hole pairs in monolayer graphene are photoexcited by a pump pulse. This is followed by a terahertz probe pulse that measures the pump-induced change in the transmission $\Delta T = T - T_0$ (red curve). The time dynamics of the photoexcited carriers is studied by varying the time delay t between the pump pulse and the probe pulse. The change in transmission ΔT, which is directly proportional to the change in terahertz conductivity, is used to characterize the degree to which secondary hot electrons are produced as the photoexcited electron cascades down to the Fermi level. **b**, Time-resolved carrier dynamics for two different photon energies: the pump-induced change in terahertz transmission $\Delta T/T_0$ as a function of pump–probe delay time t for fixed absorbed photon density $N_{photon} \sim 0.1 \times 10^{12}$ cm^{-2}. The insets show a schematic representation of the carrier distribution $N(\epsilon)$ before ($t < 0$) and long after ($t \gg \tau_{peak}$) pump excitation, and the hottest carrier distribution $N^*(\epsilon)$ directly after the energy relaxation cascade ($t = \tau_{peak}$). **c**, Scaling of the differential transmission signal $\Delta T/T_0$ peak values, obtained from the time traces as in **b** at $t = \tau_{peak}$ for six photon energies as a function of absorbed photon density N_{photon}. The lines are linear fits to guide the eye, showing that the signal increases linearly with absorbed photon density. For a given absorbed photon density N_{photon} a higher photon energy hf leads to an increased signal, corresponding to a hotter carrier distribution. **d**, The effect of varying hf on the energy cascade illustrated for two photon energies, $hf' > hf$. Photoexcitation creates a primary electron–hole pair (grey and orange sphere), and triggers a cascade of carrier–carrier scattering steps, where energy is transferred to multiple secondary hot electrons in the conduction band (orange spheres excited to red spheres), generating a hot carrier distribution. The number of secondary hot electrons increases with photon energy, leading to a hotter carrier distribution and a larger observed $\Delta T/T_0$ signal.

a fixed pump wavelength to study charge dynamics in multilayer graphene[13–18], and with a variable pump wavelength to study the effects of carrier–carrier interaction in semiconductor materials[8,9,11]. Here we apply this technique with variable pump wavelength to examine the energy relaxation cascade of photoexcited carriers in graphene. We use a monolayer of intrinsically doped graphene, in contrast to previous optical pump–terahertz probe studies that used multilayer (undoped) graphene[13–18]. We find that the photoexcited density of carriers with energy above the Fermi energy scales linearly with photon energy (for constant absorbed photon density). Notably, this scaling is found over a wide range that spans almost an order of magnitude in photon wavelength. The linear scaling indicates that carrier–carrier scattering is remarkably efficient, in good agreement with our results from a theoretical model that considers electron–electron scattering and electron–optical-phonon scattering.

The intrinsically doped graphene sample that we use for our study consists of a monolayer of graphene (grown by chemical vapour deposition) transferred onto a quartz substrate. From Raman spectroscopy we estimate a Fermi energy of $\mu \sim 0.17 \pm 0.05$ eV, which corresponds to an intrinsic carrier concentration of $\sim 2 \times 10^{12}$ carriers cm^{-2}. We further characterize the sample using terahertz transmission (without optical excitation) and find that the graphene monolayer has a spectrally flat absorption of ~5% in the 0.4–1.6 THz region. This absorption is due to intraband momentum scattering of the intrinsic carriers (Drude conductivity) with an extracted average transport time of $\tau_{tr} \sim 20$ fs (see Supplementary Information for a detailed sample characterization).

Our method for probing the energy relaxation dynamics of photoexcited carriers is illustrated in Fig. 1a. We optically excite the graphene/quartz stack and examine the pump-induced change in terahertz transmission $\Delta T = T - T_0$, where T and T_0 are the transmission with and without photoexcitation, respectively. ΔT was measured by the attenuation of the terahertz electric field. The terahertz pulses follow the pump pulses after a tunable time delay with a time resolution of ~100 fs. As the graphene layer is thin, the change in transmission is directly related to the photoconductive response so that $\Delta T/T_0 \propto -\Delta\sigma$ (see Supplementary Information). Here $\Delta\sigma$ is the pump-induced change in the terahertz conductivity, which we refer to as the terahertz photoconductivity.

The essential features of the observed dynamics are exemplified by two typical differential transmission time traces shown in Fig. 1b. The observed temporal evolution is non-monotonic: the differential transmission first rises in an approximately linear fashion, reaching a peak at a delay time $\tau_{peak} \sim 200$ fs, and finally decays on a longer timescale ~1.4 ps. These observations can be explained as

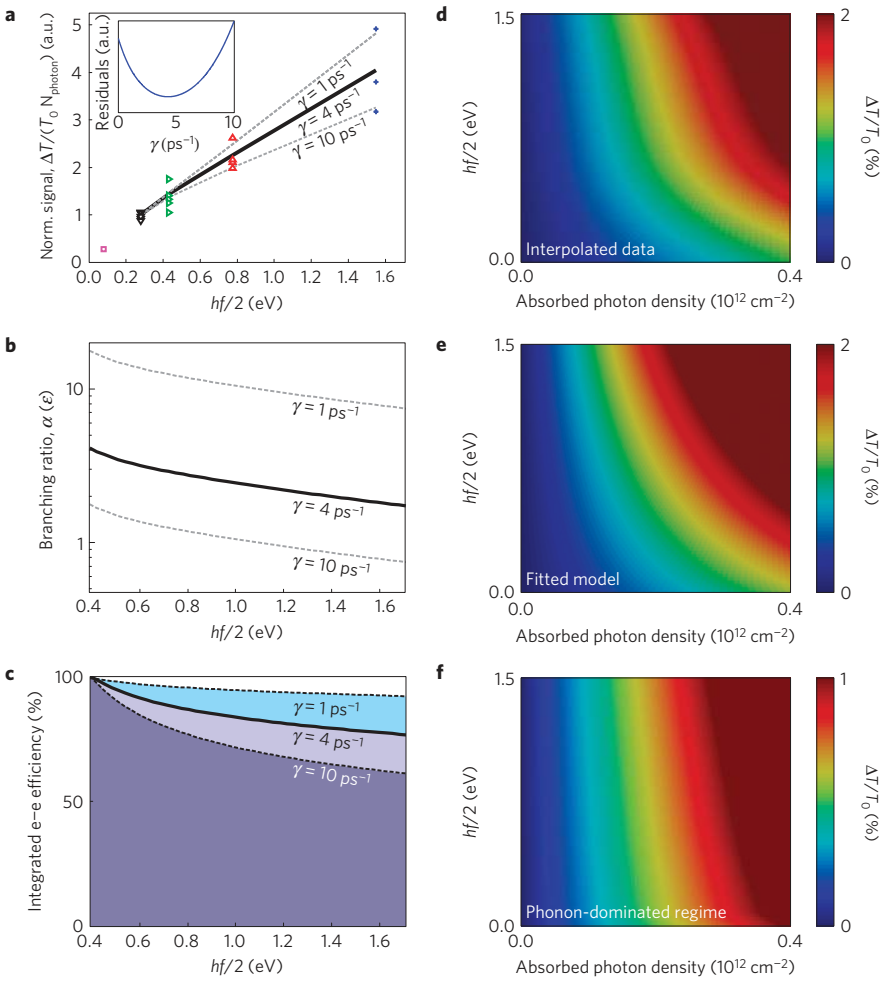

Figure 2 | Carrier–carrier scattering efficiency. a, Extraction of the branching ratio between electron–electron scattering and optical-phonon emission from comparison of the experimental data and model: the pump–probe signal $\Delta T/T_0$ peak value normalized by absorbed photon density N_{photon} features approximately linear scaling with hf, indicating that electron–electron scattering dominates the energy relaxation cascade (see text). Deviation from linearity is accounted for in the model by including optical-phonon emission with a coupling strength γ (see equation (1)). The best-fit curve (solid line) and the curves that marginally agree with the experimental data (dashed lines) are shown. The inset shows the fit residuals. **b**, The branching ratio (see equation (2)) for the ca rrier–carrier scattering and optical-phonon emissions pathways as a function of initial carrier energy for the three coupling strengths shown in **a**. Values larger than 1 indicate that electron–electron scattering is the dominant energy-relaxation pathway. **c**, The integrated efficiency for the carrier–carrier scattering pathway (see equation (3)) as a function of initial carrier energy for the same three coupling strength values: best-fit (solid line), and upper and lower bounds. The estimated efficiencies are well above 50%, indicating that a large fraction of incident photon energy is transferred to the electronic system through efficient carrier–carrier scattering. **d**–**f**, Bird's eye view of the differential signal versus photon energy and absorbed photon number density for experimental data (**d**), model best-fit (**e**) and (simulated) phonon-emission-dominated cascade (**f**). For efficient carrier–carrier scattering, the differential transmission signal is expected to increase with both absorbed photon density N_{photon} and with initial carrier energy $hf/2$. The contour lines of constant $\Delta T/T_0$ as a function of N_{photon} and $hf/2$ obtained by interpolation of the data (**d**) indeed show this behaviour. The good overall correspondence with the model for a best-fit γ value (**e**) further corroborates the conclusion that electron–electron scattering dominates the cascade. In contrast, simulation of phonon-emission dominated cascade ($\gamma = 100$ ps^{-1}, **f**) shows significant departure from the data.

follows. During the initial rise, $t \lesssim \tau_{peak}$, carrier–carrier scattering between the photoexcited carriers and the carriers in the Fermi sea promotes carriers from below to above the Fermi level (see middle inset of Fig. 1b). Thus, the effective temperature of the carrier distribution increases, peaking at $t \approx \tau_{peak}$ when the photoexcited carriers have relaxed and a hot-carrier distribution is established. Subsequent relaxation occurs owing to electron–lattice cooling, which is a relatively slow process with a characteristic timescale ($\sim$1.4 ps) much greater than τ_{peak}. These dynamics are very similar to those observed in earlier optical pump–terahertz probe studies on multilayer (undoped) graphene[13–18].

The measured change in transmission $\Delta T/T_0$ is positive, meaning that the conductivity is reduced as a result of photoexcitation, $\Delta\sigma < 0$. The observation of negative photoconductivity is in agreement with recent terahertz pump–probe studies on monolayer graphene[19,20]. The reduction in conductivity is naturally related to secondary hot-carrier excitation processes: as the momentum scattering time $\tau_{tr}(\epsilon)$ increases with carrier energy ϵ (refs 21–23), the creation of a hot-carrier distribution after photoexcitation leads to a change in the real part of conductivity that has a negative sign (see Supplementary Information). In contrast, for multilayer (undoped) graphene a positive change in the conductivity was observed, because in that case photoexcitation leads to additional electron–hole pairs in the conduction band[13–18].

Key insight into the processes contributing to the energy relaxation cascade comes from examining how the differential transmission signal $\Delta T/T_0$ peak value scales with the photon energy hf, which in our experiment is varied over a wide range,

from the infrared (0.16 eV) to the ultraviolet (4.65 eV). As the initial photoexcited carrier energy $hf/2$ determines where the cascade begins, we can track how the photoexcited carriers relax at each stage of the energy redistribution process. As a first step, we analyse the dependence of the $\Delta T/T_0$ peak value on absorbed photon density N_{photon} (that is, the number of absorbed photons per unit of area), which is shown in Fig. 1c, for six different photon wavelengths. In the fluence regime employed here, the signal increases linearly with absorbed photon density for each photon energy. The linear dependence of terahertz photoconductivity on fluence at fixed photon energy indicates that in this regime each photoexcited carrier acts independently from the other photoexcited carriers.

Proceeding with the analysis we observe that increasing the photon energy at a fixed absorbed photon density leads to a larger differential transmission signal at the peak. This is clear from the slopes in Fig. 1c that increase with photon energy. The origin of the increased signal for increased photon energy (at fixed absorbed photon density) is shown schematically in Fig. 1d. Here, increasing the photon energy leads to an increased number of electron–electron scattering events during the relaxation cascade and thus a hotter carrier distribution. In Fig. 2a we show the effect of increasing the photon energy by plotting the peak differential transmission signal normalized by absorbed photon density. Notably, the normalized signal scales approximately linearly with the photon energy, whereas energy relaxation through phonon emission would lead to a normalized signal that would be independent of photon energy.

It is instructive to combine these observations in a unified picture that provides an intuitive bird's eye view of the energy relaxation cascade. We do this by plotting the interpolated experimental contours for the $\Delta T/T_0$ peak value as a function of photon energy and photon number (see Fig. 2d). Strikingly, the contours of constant $\Delta T/T_0$ bunch up at high photon energy and spread out at low photon energy. This confirms that the two ways to achieve a hotter distribution of carriers—either by increasing the absorbed photon density or by increasing the photon energy—are completely interchangeable. The hyperbolical shape also indicates that the differential transmission signal scales with the fluence (incident energy per area, $N_{\mathrm{photon}} \times hf$). This constitutes a clear qualitative signature of the dominance of carrier–carrier scattering. Without carrier–carrier scattering, the magnitude of the response would be determined only by the absorbed photon density, and not the excitation energy; the contour lines would have been essentially vertical, with no change in $\Delta T/T_0$ as photon energy is varied (see also Fig. 2f). From these bird's eye view plots we conclude that carrier–carrier scattering plays an important role in the energy relaxation cascade. Below we develop this notion more quantitatively and estimate the (energy dependent) efficiency of carrier–carrier scattering in graphene.

The efficiency of carrier–carrier scattering depends on the branching ratio between the two processes (carrier–carrier scattering versus electron–optical-phonon scattering) that occur during the rise stage, $0 < t \lesssim \tau_{\mathrm{peak}}$. To extract this branching ratio, we develop a simple model for energy relaxation in the photoexcitation cascade and compare it with the data. The relaxation can be described in a general form by $\mathrm{d}\epsilon/\mathrm{d}t = -\mathcal{J}_{\text{el-el}}(\epsilon) - \mathcal{J}_{\text{el-ph}}(\epsilon)$, where ϵ is the photoexcited carrier energy and $\mathcal{J}_{\text{el-el}}$ and $\mathcal{J}_{\text{el-ph}}$ represent the energy relaxation rates for the two processes. Our analysis relies on the fact that the characteristic time of the photoexcitation cascade starting at the photon energy $\epsilon = hf/2$ (at $t = 0$) and ending at the Fermi energy $\epsilon \approx \mu$ (at $t = \tau_{\mathrm{peak}}$) is much longer than the carrier–carrier scattering time. Indeed, typical values $\tau_{\mathrm{peak}} \sim 200$ fs measured in our experiment (Fig. 1b) are considerably longer than the reported values for carrier–carrier scattering times, which are well below 100 fs (refs 13,24). Thus, the electron subsystem during the cascade can be described using an effective electron temperature that is distinct from the lattice temperature. Thermal equilibration with the lattice in graphene is slow[25–27], and in our sample takes ~1.4 ps (independent of photon energy and fluence in the regime considered here). This separation of timescales allows us to describe the electronic system using the electron temperature approximation.

Carrier–carrier scattering in graphene leads to the creation of secondary hot electrons that originate from the conduction band. These secondary hot electrons give a negative contribution to the terahertz photoconductivity, because the momentum scattering time $\tau_{\mathrm{tr}}(\epsilon)$ increases with carrier energy ϵ (refs 21–23). Accounting for fast thermalization of the secondary carriers, the net change in the terahertz photoconductivity can be expressed as $-2aN_{\mathrm{photon}}\mathcal{J}_{\text{el-el}}$, where N_{photon} is the absorbed photon density, and the pre-factor a is estimated in the Supplementary Information (the factor of 2 accounts for two carriers (electron and hole) produced per photon). Integrating over the cascade, we obtain the conductivity at the peak:

$$\begin{aligned}\Delta\sigma &\approx -2N_{\mathrm{photon}}\int_{t_0}^{t_0+\tau_{\mathrm{peak}}} \mathrm{d}t a\mathcal{J}_{\text{el-el}} \\ &= -2N_{\mathrm{photon}}\int_{0}^{hf/2} \mathrm{d}\epsilon \frac{a\mathcal{J}_{\text{el-el}}(\epsilon)}{\mathcal{J}_{\text{el-el}}(\epsilon)+\mathcal{J}_{\text{el-ph}}(\epsilon)} \end{aligned} \quad (1)$$

In the case that electron–electron scattering processes dominate, $\mathcal{J}_{\text{el-el}} \gg \mathcal{J}_{\text{el-ph}}$, equation (1) directly leads to linear scaling. In this case, because a is approximately energy independent (see Supplementary Information), we have $\Delta\sigma \approx -aN_{\mathrm{photon}}hf$, that is, perfectly linear scaling. In a more realistic regime, when $\mathcal{J}_{\text{el-el}} \sim \mathcal{J}_{\text{el-ph}}$, the terahertz photoconductivity in equation (1) is sensitive to the branching ratio of the two processes,

$$\alpha(\epsilon) = \mathcal{J}_{\text{el-el}}/\mathcal{J}_{\text{el-ph}} \quad (2)$$

Using $\mathcal{J}_{\text{el-el}}$ from electron–electron scattering events described in ref. 24 and writing $\mathcal{J}_{\text{el-ph}} = \gamma(\epsilon - \omega_0)\Theta(\epsilon - \omega_0 - E_{\mathrm{F}})$ we obtain the branching ratios plotted in Fig. 2b. Here ω_0 is the optical-phonon energy (0.2 eV), Θ is a step function and γ (in $(\mathrm{ps})^{-1}$) is the coupling constant between electrons and optical phonons, which we use as a fitting parameter to obtain the branching ratio. As other Auger processes such as interband relaxation of carriers are blocked kinematically[28], $\mathcal{J}_{\text{el-el}}$ from intra-band electron–electron scattering captures the relevant carrier–carrier scattering processes. The branching ratio has a strong energy dependence (approximately $\propto 1/\epsilon$ at high energies) allowing us to use the scaling of $\Delta\sigma$ with photon energy as a sensitive probe of the magnitude of the branching ratio. Indeed, $\Delta\sigma/N_{\mathrm{photon}}$ from equation (1) begins to deviate from linear scaling (with hf) significantly when the branching ratio becomes smaller than unity, $\alpha(\epsilon) < 1$.

In Fig. 2a, we compare equation (1) for three values of the electron–phonon coupling constant γ to our observed differential transmission signal normalized by absorbed photon density (see Supplementary Information). The best-fit value $\gamma \approx 4\,\mathrm{ps}^{-1}$ corresponds to the solid curve in Fig. 2a. The branching ratio values indicate that electron–electron scattering dominates the energy relaxation cascade. For stronger electron–phonon coupling, that is, larger values of γ, we find that $\Delta\sigma$ from equation (1) bends down at higher energies, significantly deviating from linearity, as illustrated by the dotted curve for $\gamma = 10\,\mathrm{ps}^{-1}$. We can exclude fits with $\gamma > 10\,\mathrm{ps}^{-1}$ as the data clearly lie in the range $1\,\mathrm{ps}^{-1} \lesssim \gamma \lesssim 10\,\mathrm{ps}^{-1}$. Inspecting the branching ratios that correspond to $\gamma = 1$, 4 and $10\,\mathrm{ps}^{-1}$ (Fig. 2b) we conclude that the energy relaxation cascade that produces our observed $\Delta T/T_0$ has a branching ratio $\alpha(\epsilon) \gtrsim 1$. Hence, electron–electron scattering dominates the energy relaxation cascade of photoexcited carriers, prevailing over electron–optical-phonon scattering.

We find good agreement between our experimental observations and values predicted by the model. First, the branching ratio we

find in Fig. 2b is in good agreement with the theoretically predicted branching ratio. Using the known value of the electron–optical-phonon deformation potential[25], we compute $\gamma = 1.36\,\mathrm{ps}^{-1}$ (see Supplementary Information), which lies in the range of the γ values obtained by fitting the data. In the Supplementary Information we also show that the experimentally observed magnitude of the signal is in reasonable agreement with the theoretical result for a based on the effective temperature model. Furthermore, it is interesting to note that the rise time of the pump–probe signal in Fig. 1b—corresponding to the time needed for the energy relaxation cascade—is longer for excitation with a higher photon energy. Although our experimental time resolution is only marginally smaller than the rise time, the variation with photon energy indicates that the observed behaviour at $t \lesssim \tau_{\mathrm{peak}}$ is not limited by time resolution. The observed dependence is in qualitative agreement with the theoretical prediction of longer cascade times at higher photon energy, where more carrier–carrier scattering events occur during the cascade[24].

Using the branching ratios plotted in Fig. 2b, we calculate the fraction of the photon energy that remains in the electronic system after the cascade (integrated electron–electron efficiency) as

$$\eta(\epsilon_{\mathrm{i}}) = \frac{1}{\epsilon_{\mathrm{i}}}\int_0^{\epsilon_{\mathrm{i}}} \frac{\alpha(\epsilon)}{\alpha(\epsilon)+1}\mathrm{d}\epsilon, \quad \epsilon_{\mathrm{i}} = hf/2 \tag{3}$$

We plot $\eta(\epsilon_{\mathrm{i}})$ for $\gamma = 1\,\mathrm{ps}^{-1} - 10\,\mathrm{ps}^{-1}$ in Fig. 2c showing that more than 50% of the photon energy remains in the electronic system even for photoexcitation energies as high as $hf = 3\,\mathrm{eV}$. This shows that carrier–carrier interaction in graphene is highly efficient. We note that our model may overestimate the efficiency at low energies, as close to the Fermi surface energy relaxation may depend on pathways that were not included in the model: acoustic phonons, flexural phonons and substrate surface phonons. However, as these processes become important only close to the Fermi surface we expect their impact on the total efficiency to be small.

For most applications the relevant figure of merit is the integrated efficiency η as it describes the fraction of light energy that is passed to the electronic system, where hot carriers can drive currents of optoelectronic systems. However, it is also interesting to examine how many hot electrons are created from a single incident photon. Our model predicts that the number of secondary hot electrons scales approximately linearly with photon energy, $N \sim (hf/2)/\mu$ (ref. 24). Taking into account the extracted efficiency of 80% for excitation with a 3 eV pump light, we find that 9 additional hot electrons are created, by getting promoted from below to above the Fermi level in the conduction band[24].

Our study sheds new light on a long-standing question about the relative importance of electron–electron scattering versus the emission of optical phonons in the energy relaxation cascade triggered by photoexcitation. Our results indicate that the transfer of energy from photoexcited carriers to electronic degrees of freedom is efficient over a wide range of frequencies (from the ultraviolet to the infrared). This sets graphene apart from conventional semiconductor systems where the frequency range is limited by the bandgap. Furthermore, the number of secondary hot electrons is expected to be highly sensitive to the doping level[24], enabling effective manipulation of the energy cascade pathways. Thus, graphene enables enhanced quantum efficiencies and tunable energy transfer over a wide spectral range.

Received 1 October 2012; accepted 23 January 2013; published online 24 February 2013

References

1. Nair, R. R. *et al.* Fine structure constant defines visual transparency of graphene. *Science* **320,** 1308 (2008).
2. Kotov, V. N. *et al.* Electron–electron interactions in graphene: Current status and perspectives. *Rev. Mod. Phys.* **84,** 1067–1125 (2012).
3. Bonaccorso, F., Sun, Z., Hasan, T. & Ferrari, A. C. Graphene photonics and optoelectronics. *Nature Photon.* **4,** 611–622 (2010).
4. Winzer, T., Knorr, A. & Malić, E. Carrier multiplication in graphene. *Nano Lett.* **10,** 4839–4843 (2010).
5. Winzer, T. & Malić, E. Impact of Auger processes on carrier dynamics in graphene. *Phys. Rev. B* **85,** 241404 (2012).
6. Gabor, N. M. *et al.* Hot carrier assisted intrinsic photoresponse in graphene. *Science* **334,** 648–652 (2011).
7. Song, J. C. W. *et al.* Hot carrier transport and photocurrent response in graphene. *Nano Lett.* **11,** 4688–4692 (2011).
8. Pijpers, J. J. H. *et al.* Assessment of carrier-multiplication efficiency in bulk PbSe and PbS. *Nature Phys.* **5,** 811–814 (2009).
9. Pijpers, J. J. H. *et al.* Carrier multiplication and its reduction by photodoping in colloidal InAs quantum dots. *J. Phys. Chem. C* **111,** 4146–4152 (2007).
10. Schaller, R. D. & Klimov, V. I. High efficiency carrier multiplication in PbSe nanocrystals: Implications for solar energy conversion. *Phys. Rev. Lett.* **92,** 186601 (2004).
11. Schaller, R. D., Agranovich, V. M. & Klimov, V. I. High-efficiency carrier multiplication through direct photogeneration of multi-excitons via virtual single–exciton states. *Nature Phys.* **1,** 189–194 (2005).
12. Ulbricht, R. *et al.* Carrier dynamics in semiconductors studied with time-resolved terahertz spectroscopy. *Rev. Mod. Phys.* **83,** 543–586 (2011).
13. George, P. A. *et al.* Ultrafast optical-pump terahertz-probe spectroscopy of the carrier relaxation and recombination dynamics in epitaxial graphene. *Nano Lett.* **8,** 4248–4251 (2008).
14. Strait, J. H. *et al.* Very slow cooling dynamics of photoexcited carriers in graphene observed by optical-pump terahertz-probe spectroscopy. *Nano Lett.* **11,** 4902–4906 (2011).
15. Winnerl, S. *et al.* Carrier relaxation in epitaxial graphene photoexcited near the Dirac point. *Phys. Rev. Lett.* **107,** 237401 (2011).
16. Breusing, M., Ropers, C. & Elsaesser, T. Ultrafast carrier dynamics in graphite. *Phys. Rev. Lett.* **102,** 086809 (2009).
17. Breusing, M. *et al.* Ultrafast nonequilibrium carrier dynamics in a single graphene layer. *Phys. Rev. B* **83,** 153410 (2011).
18. Kampfrath, T. *et al.* Strongly coupled optical phonons in the ultrafast dynamics of the electronic energy and current relaxation in graphite. *Phys. Rev. Lett.* **95,** 187403 (2005).
19. Hwang, H.Y. *et al.* Nonlinear THz conductivity dynamics in CVD-grown graphene. Preprint http://arxiv.org/abs/1101.4985 (2011).
20. Frenzel, A. J. *et al.* Observation of suppressed THz absorption in photoexcited graphene. Preprint http://arxiv.org/abs/1301.6108 (2013).
21. Nomura, K & MacDonald, A. H. Quantum Hall ferromagnetism in graphene. *Phys. Rev. Lett.* **96,** 256602 (2006).
22. Ando, T. Screening effect and impurity scattering in monolayer graphene. *J. Phys. Soc. Jpn* **75,** 074716 (2006).
23. Das Sarma, S. D., Adam, S., Hwang, E. H. & Rossi, E. Electronic transport in two-dimensional graphene. *Rev. Mod. Phys.* **83,** 407–470 (2011).
24. Song, J. C. W. *et al.* Photo-excited carrier dynamics and impact excitation cascade in graphene. Preprint http://arxiv.org/abs/1209.4346.
25. Bistritzer, R. & MacDonald, A. H. Electronic cooling in graphene. *Phys. Rev. Lett.* **102,** 206410 (2009).
26. Tse, W-K. & Das Sarma, S. D. Energy relaxation of hot Dirac fermions in graphene. *Phys. Rev. B* **79,** 235406 (2009).
27. Song, J. C. W., Reizer, M. Y. & Levitov, L.S. Disorder-assisted electron phonon scattering and cooling pathways in graphene. *Phys. Rev. Lett.* **109,** 106602 (2012).
28. Foster, M. S. & Aleiner, I. L. Slow imbalance relaxation and thermoelectric transport in graphene. *Phys. Rev. B* **79,** 085415 (2009).

Acknowledgements

We acknowledge financial support from an NWO Rubicon grant (K.J.T.), the NSS programme, Singapore (J.C.W.S.), Office of Naval Research Grant No. N00014-09-1-0724 (L.S.L.), and Fundacio Cellex Barcelona and ERC Career integration grant GRANOP (F.H.L.K.). We thank J. Versluis for technical assistance.

Author contributions

K.J.T., F.H.L.K. and M.B. conceived the experiment; K.J.T. and S.A.J. performed the experiment; K.J.T., J.C.W.S., L.S.L. and F.H.L.K. analysed and interpreted the data; J.C.W.S. and L.S.L. developed the theoretical model; A.C., A.P. and A.Z.E. prepared the sample; K.J.T., J.C.W.S., S.A.J., M.B., L.S.L. and F.H.L.K. wrote the paper.

Additional information

Supplementary information is available in the online version of the paper. Reprints and permissions information is available online at www.nature.com/reprints. Correspondence and requests for materials should be addressed to K.J.T. or F.H.L.K.

Competing financial interests

The authors declare no competing financial interests.